Macalester Journal of Physics and Astronomy

Volume 8
Issue 1 *Spring 2020*

Article 18

May 2020

SuperCDMS: Energy Calibration of a Ge HV Particle Detector

Salamong Xiong
Macalester College, sxiong2@macalester.edu

Vuk Mandic
University of Minnesota, Twin Cities, vuk@umn.edu

Matthew Fritts
University of Minnesota, Twin Cities, fritts@umn.edu

Nicholas Mast
University of Minnesota, Twin Cities, mastx027@umn.edu

Jacob Nelson
University of Minnesota, Twin Cities, nels9125@umn.edu

SuperCDMS: Energy Calibration of a Ge HV Particle Detector

Abstract

The goal of the SuperCDMS collaboration is to directly detect dark matter. Weakly Interacting Massive Particles (WIMPs) are potential candidates. To detect WIMPs, it is important to be able to predict how a Ge/Si particle detector will respond to a dark matter signal. In particular, it is necessary to calibrate the recoil energy measured by these detectors. This paper presents evidence for dark matter, a description of the detector operation, and procedures used to analyze measured data from a SuperCDMS-HV Ge particle detector using Am-241 and a PuBe neutron source. Due to high event rate, criteria were developed to remove low-quality data arising from particle interactions that occur too soon after a previous interaction. Peaks in histograms of pulse amplitudes were identified as energy peaks from the various radioactive sources, and fits of these peaks formed the basis for generating an energy calibration function. The calibration function was used to generate the calibrated energy spectrum.

Keywords

Dark Matter, Particle Detector, Energy Calibration, SuperCDMS, Cryogenic Dark Matter Search

Cover Page Footnote

I am deeply grateful to Professor Vuk Mandic for saying yes when I asked if he's willing to mentor and have me join his group for research over the summer of 2019. I want to thank Dr. Matthew Fritts and senior graduate student Nicholas Mast, for their undivided attention and patience. I want to also thank Jacob Nelson and Max Buss, those conversations about life were great. I want to thank Professor John M. Cannon, Professor Jim Doyle, and Professor Anna Williams for their continued support. And lastly, my warmest regards to the McNair Scholars program at the University of Minnesota - Twin Cities. To say I am blessed to have their support is an understatement.

SuperCDMS: Energy Calibration of a Cryogenic Ge HV Particle Detector

Salamong Xiong, Vuk Mandic, Matthew Fritts, Nicholas Mast, Jacob Nelson

Abstract

The goal of the SuperCDMS collaboration is to directly detect dark matter. Weakly Interacting Massive Particles (WIMPs) are potential candidates. To detect WIMPs, it is important to be able to predict how a Ge/Si particle detector will respond to a dark matter signal. In particular, it is necessary to calibrate the recoil energy measured by these detectors. This paper presents evidence for dark matter, a description of the detector operation, and procedures used to analyze measured data from a SuperCDMS-HV Ge particle detector using ^{241}Am and a PuBe neutron source. Due to high event rate, criteria were developed to remove low-quality data arising from particle interactions that occur too soon after a previous interaction. Peaks in histograms of pulse amplitudes were identified as energy peaks from the various radioactive sources, and fits of these peaks formed the basis for generating an energy calibration function. The calibration function was used to generate the calibrated energy spectrum.

1 Introduction

Astrophysical and cosmological studies confirm $\approx 27\%$ of the energy density in the universe is dark matter [1,2,3,4,5]. By the ΛCDM model, dark matter is essential to the evolution of the universe [6]. Weakly Interacting Massive Particles (WIMPs) are theorized by Supersymmetry as candidates for dark matter [7,8]. The past two decades of research has favored WIMPS with masses $10\,\mathrm{GeV/c^2}$ - $10\,\mathrm{TeV/c^2}$. However, Large Hadron Collider (LHC) experiments have not found these particles at these favored masses. Asymmetric dark matter and other theoretical models suggest looking for lower masses $1\,\mathrm{GeV/c^2} < \mathrm{m}_\chi < 15\,\mathrm{GeV/c^2}$ may be productive [9]. Hence experiments, such as Super Cryogenic Dark Matter Search (SuperCDMS), are now looking for lower mass WIMPs that create energy signals of 70 eV - 100 eV; this energy range correspond to the $10\,\mathrm{GeV/c^2}$ - $10\,\mathrm{TeV/c^2}$ mass range—a much more detailed explanation is beyond the scope of this paper and would require a deep dive into the theoretical and mathematical reasons.

1.1 Evidence and Characteristics of Dark Matter

Evidence for the existence of dark matter is well established in the literature [1,2,3,4,5]. Fritz Zwicky is credited as the first to hypothesize the existence or idea of dark matter. Zwicky showed that in order for the Coma cluster to have an average dispersion velocity of 1000 km/s,

the average density must be ≈ 400 times that of the observable density [1]. He concluded that some non-luminous or 'dark' matter must be accounting for the missing density (or mass). Thus he hinted at the existence of dark matter. Since Zwicky's time, studies have provided substantial evidence for the existence of dark—establishing the existence of dark matter quite well in the literature. In the following, we look at two of these studies, galactic rotational curves and the Bullet Cluster Observation.

The rotational velocity measured against the distance from the center of a galaxy is known as a rotational curve. Rotational curves are a piece of evidence for the existence of dark matter. Ordinarily we expect that the rotational velocity of a galaxy decreases as a function of distance with the relationship of $v(r) \propto \mathrm{r}^{-\frac{1}{2}}$. However, this is not the relationship observed. The 'extra' mass can be calculated using the mass-velocity equation,

$$v(\mathrm{r}) = \sqrt{\frac{\mathrm{GM(r)}}{\mathrm{r}}} \tag{1}$$

where $v(\mathrm{r})$ is the galactic rotational velocity as a function of the radius or distance from the galactic center, r. G is the universal gravitational constant, and M(r) is the mass encompassed by a sphere of radius r (mass distribution). If $v(\mathrm{r})$ and r are known, M(r) can be solved for. The integration of M(r) over the size of the galaxy can be used to determine the total mass of the galaxy. The difference between the total mass and the observable mass will yield the missing or dark matter mass. This means the observed constant curves at large distances from the galactic center, such as those shown in Figure 1 and 2, are due to unobservable mass or dark matter. It might be possible that the observed constant curves are due to other reasons, such as more intricate dynamics we don't yet understand that may or may not involve theorizing dark matter; however, it is generally accepted that the excess unobservable mass is mainly responsible for creating this phenomenon, and this is because, as we've outlined, we can just calculate the excess mass and it explains the the constant velocity.

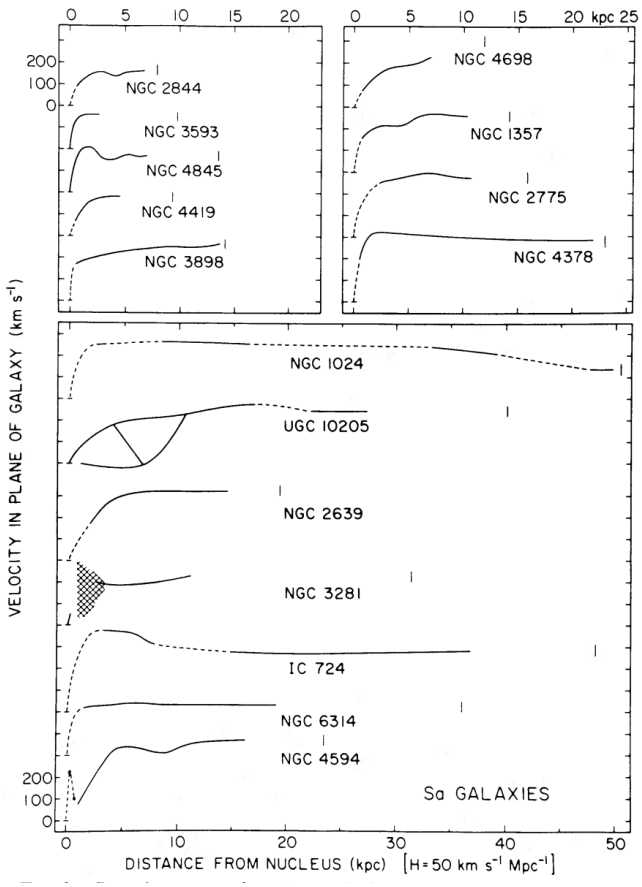

Figure 1: Rotational velocities for 16 Sa or spiral type galaxies. Retrieved from [2].

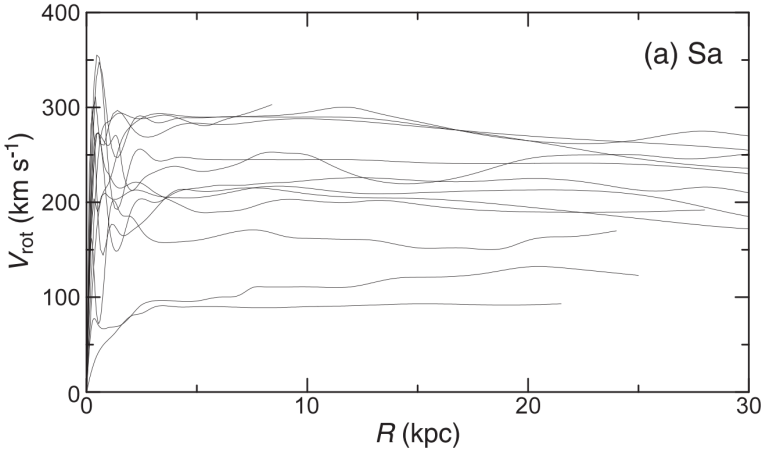

Figure 2: Recent study of several Sa or spiral type galaxies. Similar results to that of Figure 1. Retrieved from [3].

Another observation that provides evidence for the existence of dark matter is the Bullet Cluster Observation—which is the result of two clusters that collided [4]. Figure 3 can be

used to deduce where most of the mass of the Bullet Cluster is concentrated. The optical image (left) has green contours from weak gravitational lensing measurements that show the mass distribution. The X-ray image (right) shows X-ray emitting baryonic matter (log concentration amount from blue to red to yellow). When the two galactic clusters collided their ordinary matter interacted and slowed down. Using the contours, most of concentrated mass is not where the baryonic matter is; the most concentrated areas of mass are on the outer side of the cluster and are non-observable. In other words, there is a clear separation of dark and luminous matter. Thus, the Bullet Cluster serves as empirical evidence for the existence of dark matter.

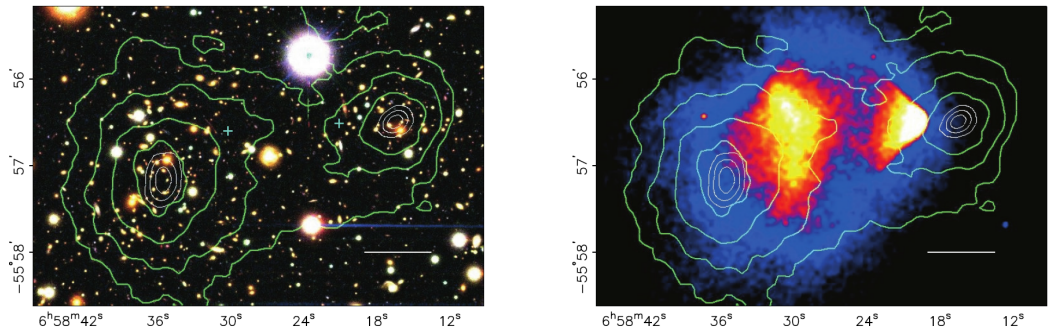

Figure 3: Optical image (left) and X-ray image (right) of the Bullet Cluster overlaid by mass distribution contours. Retrieved from [4].

Using the Bullet Cluster observation, a few characteristics of dark matter can be deduced. Dark matter has mass. It does not interact with photons or electromagnetic waves. In other words, it is electrically neutral. And it interacts minimally with itself as can be seen in Figure 3. As mentioned before, the Bullet Cluster is a result of two clusters that collided. The two clusters must have passed through each other. This collision explains the image on the right and why there are baryonic matter that are interacting with each other. If we look closely, we can see that the "core" of the two clusters or the most concentrated areas with dark matter were not disturbed on any significant scale, which suggests that dark matter interacts minimally. Clearly dark matter particles do interact with each other but how much we don't yet know, which is a part of why we say, "they interact minimally."

1.2 SuperCDMS Experiment

The goal of the SuperCDMS experiment is to directly detect dark matter [7,10]. Three generations of dark matter experiments have been conducted in the Cryogenic Dark Matter Search (CDMS) line. CDMS I was operated at Stanford University. CDMS II was operated at Soudan Underground Laboratory in Minnesota; the iron mine was converted to a lab in the 1980s. The Super Cryogenic Dark Matter Search (SuperCDMS) is the third generation and was operated in 2012 - 2015 using the same infrastructure as CDMS II and was also located at Soudan. The next iteration is located at SNOLAB, home of the Sudbury Neutrino Observatory, called "SuperCDMS SNOLAB." Each generation used larger, more sensitive detectors, and better shielded environments than its predecessors.

SuperCDMS uses Germanium (Ge) and Silicon (Si) particle detectors to directly detect WIMPs—other ways to detect WIMPs (or dark matter particles), χ, are shown in Figure 4. To detect WIMPs, it is important to be able to predict how these detectors will respond to a dark matter signal, thus requiring the creation of a calibrated recoil energy spectrum. In other words, a calibrated recoil energy spectrum can be used to identify the source of a signal, hence its importance. The energy calibration of this SuperCDMS-HV Ge detector (diameter = 100mm, thickness = 33mm) uses a ^{241}Am radioactive source and a PuBe neutron source. Analysis was conducted using the ROOT programming language developed by scientists at the European Organization for Nuclear Research (CERN).

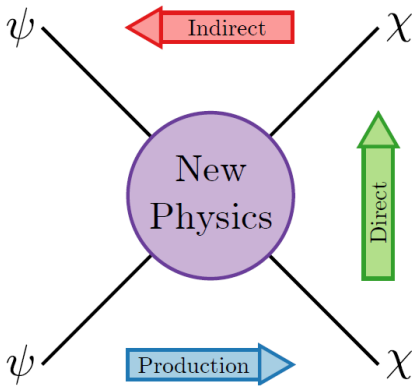

Figure 4: Feynman diagram showing possible interactions between a dark matter particle, χ, and Standard Model(SM) particle, ψ. The methods of detection are shown: production, direct, and indirect. Detection via production is by smashing two ordinary ψ particles and producing two dark χ particles, e.g. using particle accelerators. Direct is direct observation of a χ and ψ particle interaction. Indirect is looking for decay or annihilation of dark matter particles that may produce ψ. Retrieved from [10].

2 Theory and Experiment

The detector has phonon channels A, B, C, D, E, and F (Figure 5). These channels are composed of arrays of superconducting transition edge sensors (TES) that are photolithographed onto the detector surface (Figure 6). These sensors are used for measuring phonons (modes of vibration of the crystalline lattice) that arise from particle interactions or quasi-sound particles. The cryostat is cooled by a Kelvinox 100 dilution refrigerator; the fridge circulates a ^{3}He - ^{4}He mixture to reach 30 mK temperatures. Sheets of lead (Pb) and polyethylene were used for shielding against background radiation.

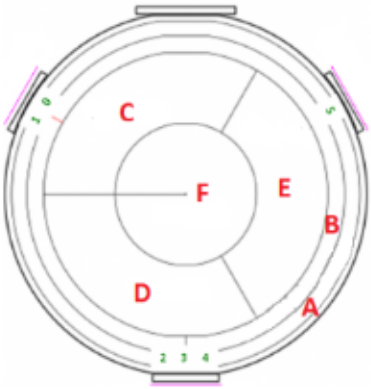

Figure 5: Layout of phonon channels of the SuperCDMS-HV Ge particle detector.

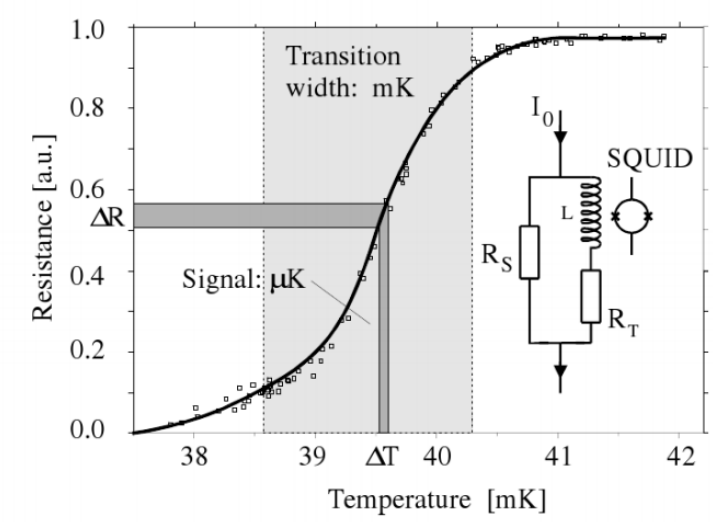

Figure 6: Example of a transition edge sensor (TES). These sensors utilize superconducting quantum interface devices (SQUIDs), which are essentially magnetometers that measure changes in a magnetic field when there's been a superconducting temperature transition. Retrieved from [11].

When a particle, χ, collides with an electron or a nucleus inside the detector, recoil phonons and electron-hole pairs are produced. An applied electric field separates the electron-hole pairs and propagates them to the surface - during the propagation, these charges interact with the crystalline lattice and produce a secondary population of phonons, known as the Neganov-Trofimov-Luke (NTL) phonons [12,13].

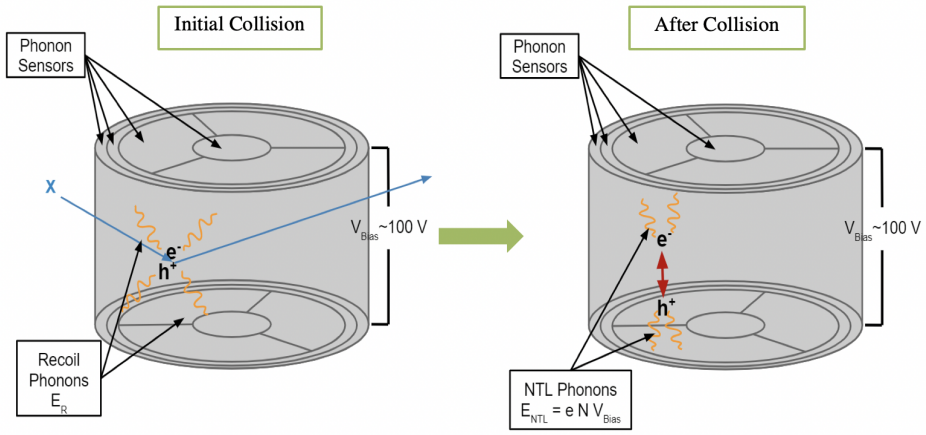

Figure 7: Collision of an unknown particle, χ, and the nucleus of a Ge target.

The total phonon energy can be calculated using,

$$E_{\mathrm{Tot}} = E_r + E_{\mathrm{NTL}} \tag{2}$$

where E_{Tot} is the total phonon energy, E_r represents the amount of energy from initial recoil phonons, and E_{NTL} represents the phonon energy produced from the electron-hole pairs and the applied voltage. E_{NTL} is defined as,

$$E_{\mathrm{NTL}} = eN_{\mathrm{e/h}}V_{\mathrm{bias}} \tag{3}$$

where e is the electron charge, $N_{e/h}$ is the number of electron-hole pairs produced, and $V_{bias} = \Delta V$ is the voltage bias or applied voltage. $N_{\mathrm{e/h}}$ is,

$$N_{e/h} = E_r/\varepsilon_{\mathrm{Ge}} \tag{4}$$

where $\varepsilon_{\mathrm{Ge}} = 3.0\,\mathrm{eV}$ is the amount of energy required to produce an electron-hole pair. Using these expressions, the total phonon energy can be rewritten as,

$$E_{Tot} = E_r\left(1 + \frac{e \times V_{bias}}{\varepsilon_{Ge}}\right) \tag{5}$$

where $\left(1 + \frac{e \times V_{bias}}{\varepsilon_{Ge}}\right)$ is a gain factor due to the NTL effect. Increasing the gain will increase the visibility of the signal in the detector—assuming that the noise remains unchanged. In this experiment, voltage was applied to achieve a constant detector bias around 130 V for 88 minutes.

The detector was exposed to ^{241}Am and a PuBe neutron source. These two sources were used for the calibration because they create known energy lines. ^{241}Am emits several prominent γ-rays at energies of: 13.95, 17.74, 26.4, and 59.54 keV. The PuBe source produces neutrons that are captured by ^{70}Ge, the ^{71}Ge then decays via electron-capture and produces X-rays and Auger electrons at energies of: 0.16, 1.3, and 10.37 keV. Other sources such as silver (Ag), gold (Au), and palladium (Pd) may show up via fluorescence—emission of high

energy electromagnetic waves due to excitation. In this experiment we only saw ^{47}Ag with an energy line of 22.162 keV. These energy lines are tabulated in Table 1.

Source	Energy Lines (keV)
Ge-71	0.16
Ge-71	1.3
Ge-71	10.37
Am-241	13.95
Am-241	17.74
Ag-47	22.162
Am-241	26.4
Am-241	59.54

Table 1: Sources and their energy lines seen in the detector.

3 Data Processing

Four quality cuts were applied to the raw data collected: "random triggers cut" , "baseline level cut" , "baseline standard deviation cut", and "pulse/integral fit." The random triggers cut remove signals that were triggered randomly—which may sometimes remove random triggers that were high quality data (Figure 8) because they were randomly triggered; the removal of randoms, however, is always more beneficial. It should be noted that the random triggers are not accidental and were taken purpose to understand the detector noise when there is no signal present.

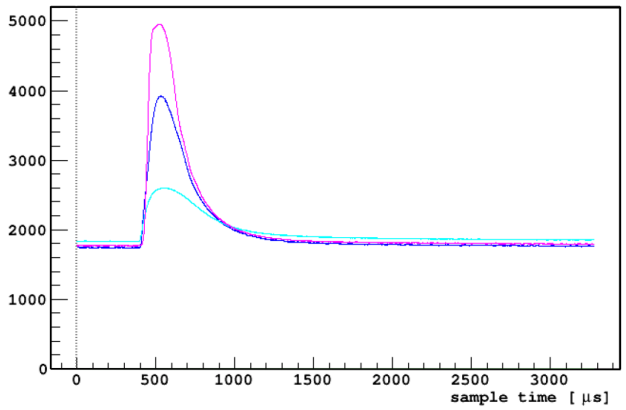

Figure 8: Example of high quality data. Pulses belong to one event seen by three different phonon channels (out of the six). On the y-axis is the digital to analog values of the total phonon energy; these values are not meaningful and have no units but show the relative strength. Analysis is required to make these values meaningful.

The baseline level cut was configured to remove raw data that had a baseline level too high or too low relative from normal ($\approx 1800 - 2000$ on the y-axis in Figures 8 and 9). The

baseline standard deviation cut was configured to remove data that had baselines that were not flat (Figure 9b); in other words, the cut removed pulse data that were coming off of the tail of another pulse. The pulse/integral fit cut was configured to remove data that had two events or pulses bunched up together like that in Figure 9a. The Optimal Filter (OF) algorithm attempts to fit a single pulse shape to these two piled-up pulses, resulting in a too large estimate of the pulse amplitude (and energy) [14]. The integral algorithm simply integrates the area under the curve of the pulse. For any good event, such as the one shown in Figure 8, the two algorithms (pulse/integral fit and OF) produce similar estimates, and the ratio pulse/integral is near unity or some other "agreement" constant that is related to the average width of the pulse. For piled-up pulses, such as those shown in Figure 9a, the ratio will be different from unity or the agreement constant, if so then it is removed from the overall data set. In a sense, these 4 quality cuts are applied to remove as much of the 9a and 9b as possible, and leaving us with mostly good data (or Figure 8).

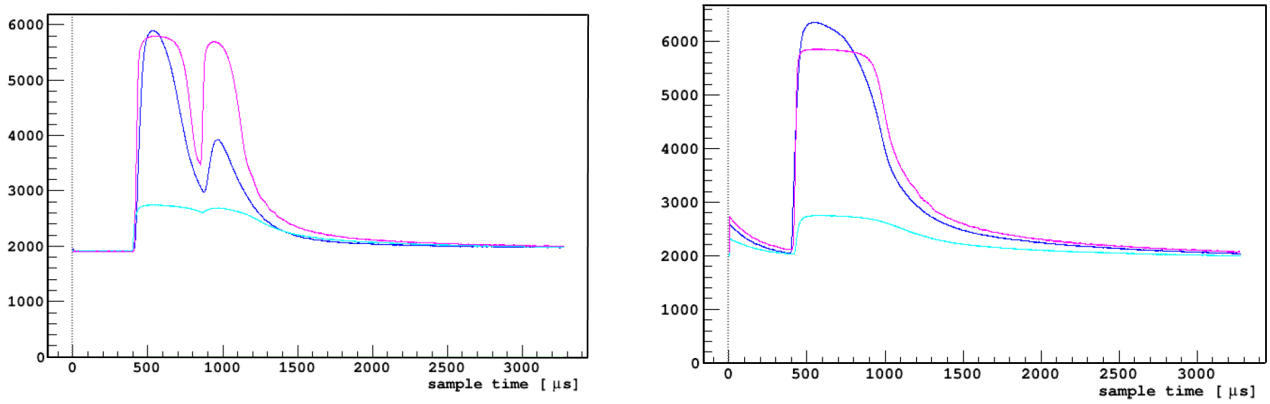

(a) (b)

Figure 9: Examples of low quality data. A high event rate will cause a pulse or energy signal to bunch up like that of (a). The optimal filter (OF) only counts (a) as a single event and will fit the two events as one. (b) is similar to (a) where the tail of another event was included. Note that the pulses (a) belong to one event seen by three different phonon channels (out of the six); the same applies for (b). Note again, that on the y-axis is the digital to analog values of the total phonon energy; these values are not meaningful and have no units but show the relative strength. Analysis is required to make these values meaningful.

4 Data Analysis & Results

Five 88-minute data series were analyzed for this energy calibration. The data was analyzed using the ROOT programming language developed by scientists at CERN.

4.1 Channel Balancing

After applying the four data quality cuts (random triggers, baseline, baseline standard deviation, pulse/integral fit), the processed raw data set needs to be balanced relative to the

center channel (Channel F, Figure 5). This is because the different channels have somewhat different linear responses to the same amount of absorbed energy. Phonon channel F (PF) was used as the reference channel due to its close proximity to the ^{241}Am sources. The raw units are essentially arbitrary and are referred to as "arb."Balancing will scale according to PF such that 1 unit in the other channels is the same as 1 unit in PF. Individual channels (A, B, C, D, & E) were multiplied by scaling factors until the ratio between each channel and PF was 1, indicating the channels were balanced (Figure 10b). Another indication that the channels were balanced properly is that of Figure 11b, where the visibility of the expected energy lines had increased. Afterward, each channel was multiplied by its respective scaling factor and added together, creating a balanced sum named Psumb.

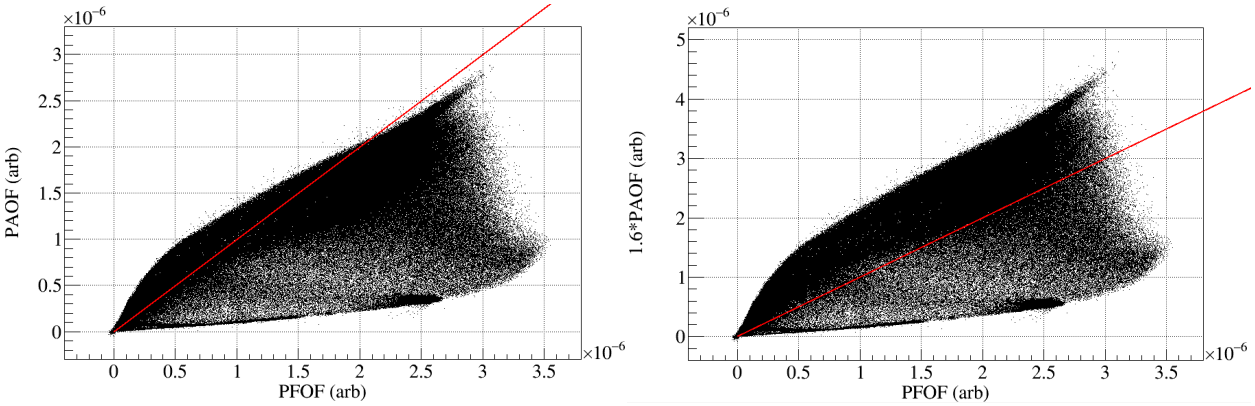

(a) (b)

Figure 10: Phonon channel A (PAOF) was plotted against phonon channel F (PFOF) for balancing, where OF is the optimal filter used for processing raw data. (a) shows an unbalanced and (b) shows a balanced PAOF. The red line drawn has a slope of 1. From (a) it is clear that PAOF should be multiplied by some factor. In this case, 1.6 is the scaling factor.

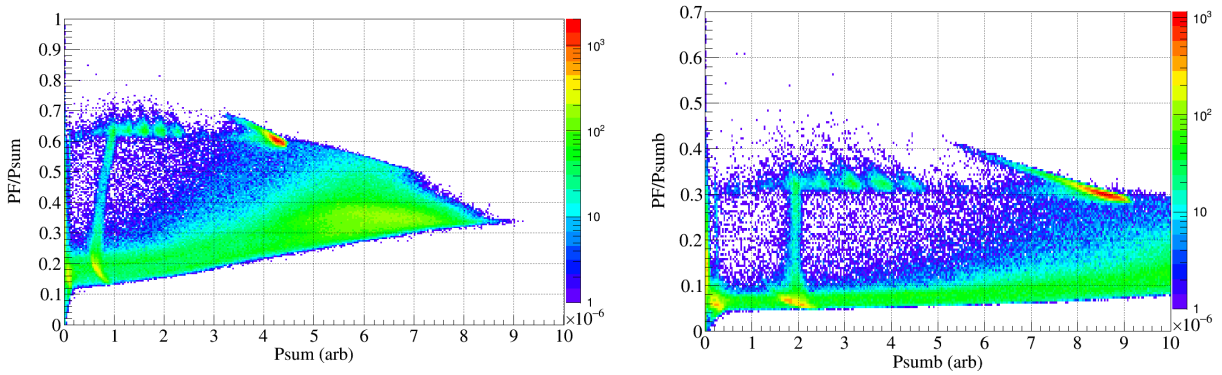

(a) (b)

Figure 11: (a) plots PF/Psum vs Psum without balancing, where Psum is the sum of the unbalanced processed data. (b) plots PF/Psumb vs Psumb where 'b' is for balanced. Data in both (a) and (b) were processed through an optimal filter algorithm and 4 quality cuts (Section 3). (b) shows that balancing is necessary for increasing the visibility of the energy features.

4.2 Calibrated Energy Spectrum

Histograms of Psumb are produced and the peaks are fitted by Gaussians (Figure 13 is an example). This determines the Psumb values that correspond to the known energies of ^{71}Ge, ^{241}Am, and ^{47}Ag (Table 1). Tight (PF/Psumb $>$ 0.28) and loose (PF/Psumb $>$ 0.20) selections were applied for determining the average Psumb value that corresponds to each energy line (Figure 11a); the determined average Psumb value are tabulated in Table 2.

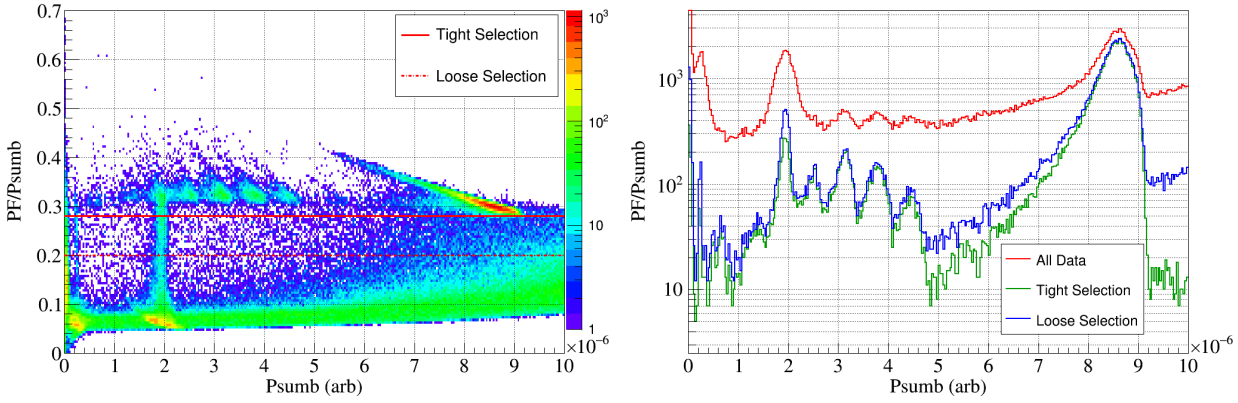

(a) (b)

Figure 12: In (a) tight (PF/Psumb $>$ 0.28) and loose (PF/Psumb $>$ 0.2) selections of processed data are indicated by full and dotted red lines respectively.(b) shows the difference in resolution between tight, loose, and all data selection. Which is important for determining the average Psumb value that correspond to the known energy lines.

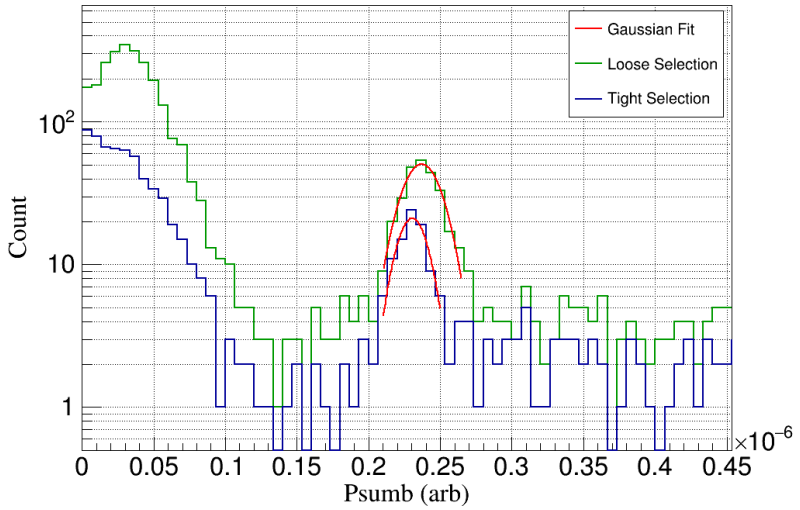

Figure 13: Example of Gaussian fits on tight and loose selections on the 1.3 keV line produced from ^{71}Ge.

Average Psumb (arb)	Energy Lines (keV)
2.34E-07	1.3
1.94E-06	10.37
2.54E-06	13.95
3.14E-06	17.74
3.77E-06	22.162
4.43E-06	26.4
8.61E-06	59.54

Table 2: Average Psumb values and keV lines.

After fitting and determining the average Psumb values that corresponds to the energy lines (Table 2), a Psumb vs keV plot was made and fitted with a quadratic equation, constrained to the origin, to determine the energy calibration function (Figure 14).

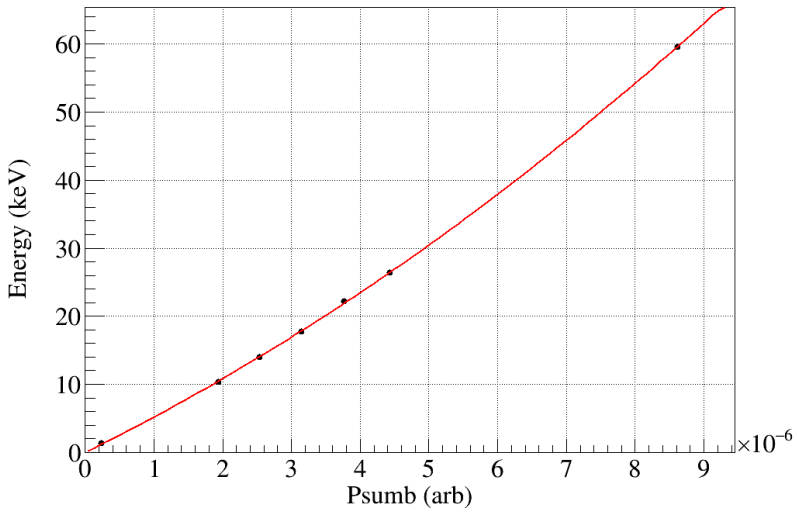

Figure 14: Average Psumb and corresponding keV values plotted and fitted.

The energy calibration function, in units of keV, was determined to be,

$$E(\text{Psumb}) = 2.28 \times 10^{11} * \text{Psumb}^2 + 4.96 \times 10^6 * \text{Psumb} \tag{6}$$

The calibration function is then used for creating the calibrated energy spectrum of the detector (Figure 15).

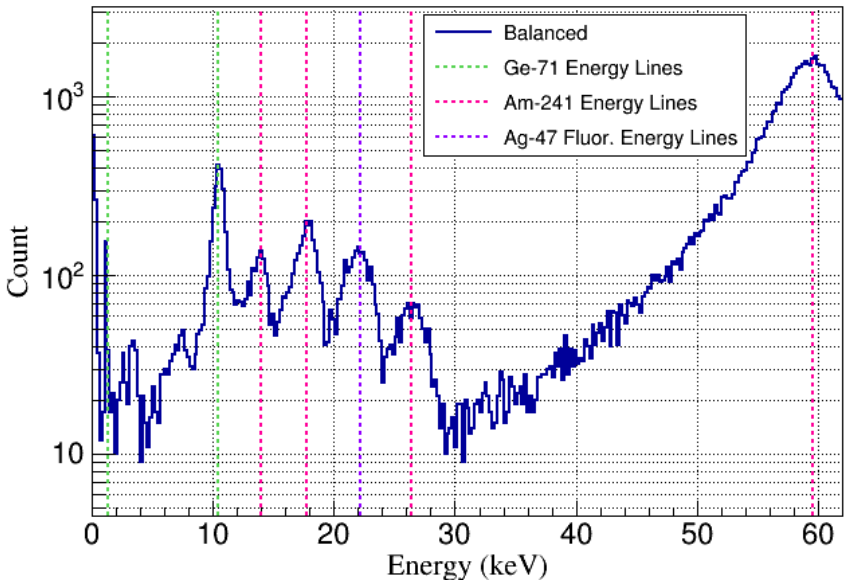

Figure 15: Calibrated energy spectrum. Energy features from the known sources are indicated by colorized dash lines. Peaks between 1.3 and 10.37 keV are not yet definitively identified.

5 Conclusion

A calibrated energy spectrum was created from analysis of five processed data series of 88 minutes for a total of 7.33 hours worth of data. In the spectrum, we were able to observe energy features above the 1.3 keV line and were able to characterize the detector's response to relatively high energy events—note that the sources of the peaks between 1.3 keV and 10.37 keV are still unidentified. This is definitely progress forward but we did not make the full progress we wanted. There is a smaller energy signal from ^{71}Ge, the 0.16 keV, that we wanted the detector to be able to see. This is because we are expecting the energy released by low-mass WIMPs collision events to be relatively low (70 eV - 100 eV); which if we calculate backwards, using known equations in [7,10], the mass will fall between the lower masses that Asymmetric dark matter and other theoretical model recommend looking for. The calibrated recoil energy spectrum allows characterization but does not yet have the statistics to see the number of small 0.16 keV events. Being able to see these events would enable recoil energy calibration at lower energies and therefore search for lower-mass WIMPs.

6 Future Work

We noticed time variations in the data (Figure 16). The time variation introduces a small time dependence in the data. A piece-wise function can be used to do a time correction but was not conducted due to time constraints. A time correction of the data in the future could also improve the calibrated energy spectrum resolution.

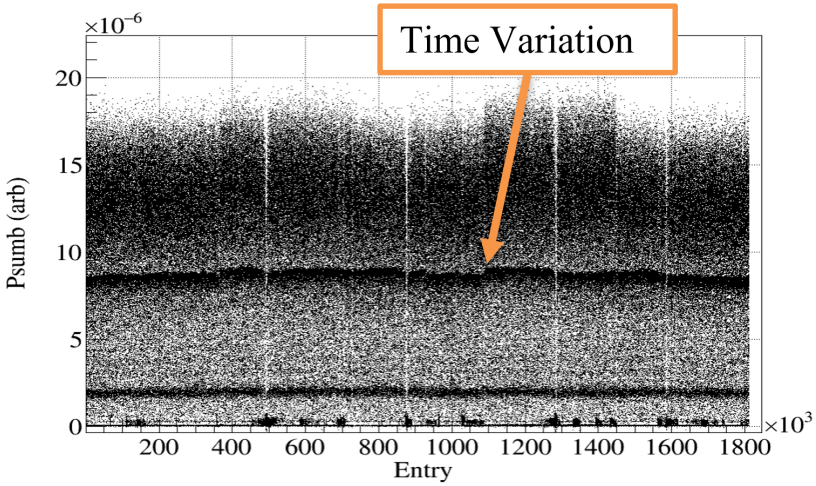

Figure 16: Shows the time variation of the data.

Recently we were able to see the 0.16 keV. In the future, this new data (additional statistics) and an in-depth study of the quality cuts for removing low-quality data could improve the resolution of the energy spectrum. And using a movable ^{241}Am source could help us understand if there is position dependence, and therefore allow us to correct the position dependence—which could improve the resolution of the energy spectrum.

References

[1] F. Zwicky, Die Rotverschiebung von extragalaktischen Nebeln, Helv. Phys. Acta 6, 110127 (1933).

[2] V. Rubin et al., "Rotation Velocities of 16 Sa Galaxies and a Comparison of Sa, Sb, And Sc Rotational Properties," Astrophys. J. 289, 81-104 (1986).

[3] Y. Sofue, "Rotational and Mass in the Milky Way and Spiral Galaxies," Astron. Soc. Japan. 69, 1-35 (2017)

[4] D. Clowe et al., "A Direct Emprical Proof of the Existence of Dark Matter," Astrophys. J. 648, L109-L115 (2006).

[5] G. Hinshaw et al., "Three-Year Wilkinson Microwave Anistropy (WMAP) Observations: Temperature Analaysis", Astrophys. J. 170, 288-334 (2007).

[6] Ryden, B. 2017, Introduction to Cosmology, Cambridge University Press, Vol 1, Tj International Ltd. Padstow Cornwall.

[7] R. Agnese, "Simulating the SuperCDMS Dark Matter Detection Response and Readout," Ph.D. Thesis, University of Florida (2017).

[8] G. Jungman, M. Kamionkowski, and K. Griest, "Supersymmetric dark matter," Phys. Rep. 267, 195-373 (1996).

[9] T. Lin, H.-B. Yu, and K. M. Zurek, "Symmetric and asymmetric light dark matter," Phys. Rev. D 85, 063503 (2012).

[10] D. Barker, "SuperCDMS Background Models for Low-Mass Dark Matter Searches," Ph.D. Thesis, University of Minnesota (2018).

[11] H. Demers, "Two facets of the X-ray Microanalysis at Low Voltage: the Secondary Fluorescence X-rays Emission and the Microcalorimeter Energy-Dispersive Spectrometer," Ph. D. Thesis, McGill University (2008).

[12] B. Neganov and V. Tromov, Otkrytia i izobretenia 146, 215 (1985).

[13] P. N. Luke, "Voltage-assisted calorimetric Ionization Detector," J. Appl. Phys. 64, 6858-6860 (1988).

[14] S. Golwala, "Exclusion Limits On the WIMP-Nucleon Elastic-Scattering Cross Section from the Cryogenic Dark Matter Search," Ph.D. Thesis, University of California - Berkeley (2000).